

## REFINED ANALYTICAL COLLAPSE CAPACITY SPECTRA \*

S. TSANTAKI<sup>1</sup>, L. WURZER<sup>2</sup>, C. JÄGER<sup>3</sup>, C. ADAM<sup>4\*\*</sup> AND M. OBERGUGGENBERGER<sup>5</sup>

<sup>1,3,4</sup>Unit of Applied Mechanics, University of Innsbruck, Technikerstr. 13, 6020 Innsbruck, Austria  
Email: christoph.adam@uibk.ac.at

<sup>2,5</sup>Unit of Engineering Mathematics, University of Innsbruck, Innsbruck, Austria

**Abstract**– Recently, two of the authors have introduced the collapse capacity spectrum methodology, which allows the assessment of the collapse capacity of highly inelastic P-delta sensitive regular frame structures without performing non-linear time-history analyses. The main ingredient of this method is the collapse capacity spectrum, which represents the seismic collapse capacity of an inelastic non-deteriorating single-degree-of-freedom system vulnerable to the P-delta effect as a function of its initial period, negative post-yield stiffness ratio, viscous damping coefficient, and the shape of the hysteretic loop. In the present study, multiple linear regression analyses are applied to provide enhanced analytical expressions of these spectra. The record-to-record uncertainty of the collapse capacity is captured through median, 16th and 84th percentile spectra. For several test systems analytical collapse fragility functions based on these spectra are set in contrast with the corresponding sorted individual collapse capacities. These examples prove the superiority of the proposed analytical expressions compared to its original formulation.

**Keywords**– Collapse capacity spectrum, dynamic instability, P-delta effect, regression analysis

### 1. INTRODUCTION

A modern engineered building located in an earthquake environment must be provided with an adequate margin of safety against structural collapse during extreme earthquakes. This primary goal of earthquake engineering can be accomplished only if tools for predicting seismic collapse with sufficient confidence are well understood, readily available and easy to apply in engineering practice. Prediction of collapse includes appropriate specification of the seismic hazard, identification of possible modes of collapse, structural modeling, and application of reliable mathematical procedures within a probabilistic framework to capture both record-to-record and modeling uncertainties. Past catastrophic earthquakes have shown that for a building the predominant mode of collapse is sidesway collapse, which may be the consequence of successive reduction of the lateral load bearing capacity due to cyclic component deterioration. Highly inelastic flexible buildings subjected to second-order P-delta effects may exhibit a negative lateral post-yield stiffness. In such a situation sidesway collapse is attained at a rapid rate if the ground motion is sufficiently severe to drive the structure into its inelastic branch of deformation [1]. However, in many buildings only the interaction of cyclic component deterioration and P-delta lead to sidesway collapse [2].

This paper discusses only one out of various aspects of this complex problem, i.e. prediction of the seismic (sidesway) collapse capacity of highly inelastic single-degree-of-freedom (SDOF) systems vulnerable to the destabilizing effect of gravity (P-delta effect) with simplified measures. Fundamental studies on seismic collapse of this type of systems can be found in [3-5]. Miranda and Akkar [6] provide an empirical equation to estimate the minimum lateral strength up to which P-delta induced collapse of

---

\*Received by the editors April 4, 2014; Accepted June 16, 2015.

\*\*Corresponding author

SDOF systems is prevented. Based on this study, Vamvatsikos et al. [7] study the dynamic instability of SDOF systems with nontrivial backbone curves. Asimakopoulos et al. [8] propose a simple formula for a yield displacement amplification factor as a function of the ductility and the stability coefficient. Villaverde [9] provides a thorough survey on studies dealing with collapse assessment of earthquake-excited structures.

Despite the fact that SDOF systems are the simplest systems of structural dynamics, they provide the basis for the practical seismic response analysis of first mode dominated multi-degree-of-freedom (MDOF) buildings. In this respect, equivalent SDOF systems in combination with elastic and inelastic spectra developed in various forms are the main tools of both strength-based and the displacement-based evaluation and design methodologies [10]. Borrowing this concept, Adam and Jäger [11] have recently developed the collapse capacity spectrum methodology for assessing the global sidesway collapse capacity of P-delta sensitive regular frame structures, based on bilinearized global pushover curves of the structure with and without considering gravity loads, an equivalent SDOF system, and a collapse capacity spectrum. This method allows a quick and yet accurate assessment of the collapse capacity avoiding computational expensive non-linear time-history analyses. For details refer to [12-14].

The main ingredient of this methodology is the collapse capacity spectrum, where the relative collapse capacity of a non-degrading inelastic SDOF system is represented as a function of the initial structural period, the normalized negative post-yield stiffness, the viscous damping coefficient, and the assigned hysteretic cyclic behavior [12]. Capturing the record-to-record variability have derived collapse capacity spectra for various records of three different sets of ground motions, and subsequently evaluated them statistically [12] and [14]. As an outcome of the regression analyses analytical expressions for median, 16th and 84th percentile collapse capacity spectra – so-called design collapse capacity spectra – are now available. However, for very stiff as well as for very flexible structures these analytical collapse capacity spectra do not approximate with sufficient accuracy the actual collapse capacity. In particular, analytical 16th and 84th percentile spectra deviate from the underlying numerically derived statistical collapse capacity quantities. Furthermore, (although only of academic interest) for rigid systems, where the collapse capacity is a record-independent deterministic quantity depending only on structural parameters, these analytical expressions do not render the true collapse capacity.

Thus, the objective of the present paper is to provide a set of refined analytical collapse capacity spectra, representing a “best-fit” of the underlying median, 16th, and 84th percentile collapse capacities. To meet this objective several multiple regression analyses are performed with the statistically evaluated collapse capacity as independent variable, and three regressors, i.e. the structural period of vibration, the damping coefficient, and the negative post-yield stiffness ratio. The improvement compared to the original formulation is assessed with an appropriate measure of error, which also gives information about the goodness of fit of the approximation [12].

## 2. COLLAPSE CAPACITY SPECTRA – STATE OF THE ART

### *a) Collapse capacity of an inelastic SDOF system vulnerable to P-delta*

In the inelastic non-deteriorating SDOF system of Fig. 1a the gravity load generates a shear deformation of its hysteretic force-displacement relationship as shown in Fig. 1b. Characteristic displacements (such as the yield displacement) of this relationship remain unchanged, whereas the characteristic forces (such as the strength) are reduced. As a result, the slope of the curve is decreased in its elastic and post-elastic branch of deformation. The magnitude of this reduction can be expressed by means of the stability coefficient  $\theta$ , which is, for the system of Fig. 1a, a function of the gravity load  $P$ , length  $h$ , and rotational stiffness  $k_r$  [12],

$$\theta = \frac{Ph}{k_r} \tag{1}$$

As a showcase Fig. 1b visualizes the P-delta effect on the non-dimensional hysteretic behavior of an SDOF system with non-deteriorating bilinear characteristics [5], where the restoring force  $f$  is normalized with respect to the yield strength  $f_y$ , and the tip displacement  $x$  is divided by the displacement at the onset of yield  $x_y$ . In this example the post-yield stiffness is negative, because the stability coefficient  $\theta$  is larger than the hardening ratio  $\alpha$ .

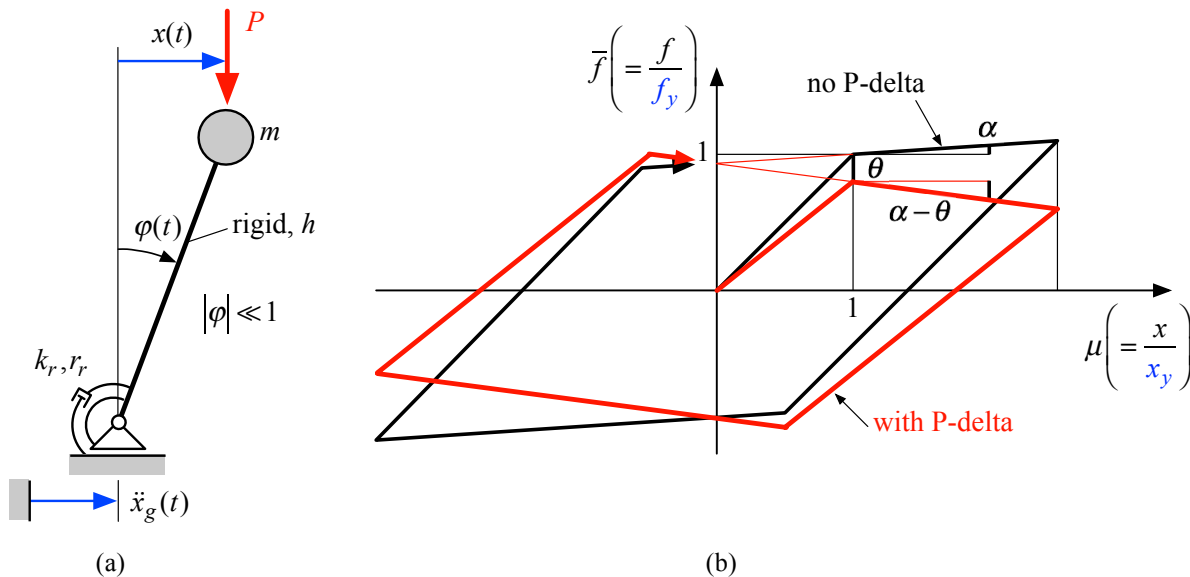


Fig. 1. (a) Mechanical model of an SDOF system subjected to gravity and earthquake excitation. (b) Normalized bilinear cyclic structural behavior with and without the destabilizing effect of gravity loads [12]

A negative slope of the post-tangential stiffness, expressed by the difference of the stability coefficient  $\theta$  and the strength hardening coefficient  $\alpha$  (i.e.  $\theta - \alpha$ ), is the essential condition that the structure may collapse under severe earthquake excitation. In [13] it is proven that for given excitation collapse of inelastic non-deteriorating SDOF systems vulnerable to P-delta is governed by the following structural parameters:

- The elastic structural period of vibration  $T$ ,
- the negative slope of the post-tangential stiffness  $\theta - \alpha$  ( $0 \leq \alpha \leq 0.06$ ,  $T \geq 0.1s$ ),
- the viscous damping coefficient  $\zeta$  (usually taken as 5%), and
- the shape of the hysteretic loop, i.e. the normalized force – displacement relation  $\bar{f} - \mu$ .

The collapse capacity - defined as the maximum ground motion intensity at which the structure still maintains dynamic stability [2] - of an inelastic SDOF system vulnerable to P-delta is a function of these structural parameters and the particular earthquake record, which excites this system to vibrations. Most generally, the collapse capacity is determined based on incremental dynamic analysis (IDA) [15]. Thereby, non-linear time-history analyses are performed for a specific earthquake record incrementing its intensity repeatedly up to collapse.

In the study of [12], which serves as basis of the present investigation, the relative collapse capacity of a P-delta vulnerable SDOF system subjected to a ground motion record (denoted by index  $i$ ) is based on the non-dimensional ratio of 5%-damped spectral acceleration at the structure's fundamental period  $S_{a,i}(T, \zeta = 0.05) / g$  to the base shear coefficient  $\gamma$ ,

$$CC_i = \frac{S_{a,i}}{g\gamma} \Big|_{collapse}, \quad \gamma = \frac{f_y}{mg} \quad (2)$$

$m$  the mass of the SDOF system, and  $g$  denotes the acceleration of gravity.

The inherent record-to-record variability leads to different collapse capacity for each ground motion record. Thus, the collapse capacity is not only derived for one record but for a set of carefully compiled representative ground motions. The collapse fragility curve, which represents aleatory uncertainty due to record-to-record variability, is obtained by ordering the individual collapse capacities  $CC_i$  [9]. Ibarra and Krawinkler [16, 17] provide good arguments that the individual collapse capacities are more or less log-normally distributed. Since a log-normal distribution is characterized by the median and the 16th and 84th percentiles, the median (referred to as  $CC_{P50}$ ), and the 16th and 84th percentiles (denoted as  $CC_{P16}$  and  $CC_{P84}$ , respectively) of the individual collapse capacities are determined. Then, the assumption of a log-normal distribution allows a reasonable approximation of collapse fragility curves based only on these statistical quantities [16].

For rigid systems (i.e. systems with periods  $T = 0$ ) the collapse capacity is record independent, and given by the deterministic expression [14]

$$CC(T = 0) = 1 - \theta \quad (3)$$

because the P-delta effect reduces the structural strength  $f_y$  to  $f_y(1 - \theta)$ . Eq. (3) is found from the geometrically linearized form of the equation of motion of the SDOF system (as specified in [12]) considering that the spectral acceleration  $S_a$  at period  $T = 0$  is equal to the PGA (peak ground acceleration  $\max|\ddot{x}_g|$ ). However, since the difference between the stability coefficient  $\theta$  and the hardening coefficient  $\alpha$  (i.e.  $\theta - \alpha$ ) is a governing collapse parameter for  $T \geq 0.1s$  [13], in an engineering approach for rigid systems the collapse capacity is subsequently approximated by

$$CC(T = 0) \approx 1 - (\theta - \alpha) = 1 - \theta + \alpha, \quad \alpha \leq 0.06 \quad (4)$$

Consequently, the structural parameters as specified above govern the collapse capacity in the entire period range.

### b) Collapse capacity spectra - definition

The representation of the collapse capacity of an SDOF system with assigned damping parameter  $\zeta$ , assigned negative post-yield stiffness ratio  $\theta - \alpha$ , and a particular hysteretic loop as a function of the initial structural period  $T$  is referred to as collapse capacity spectrum for a particular ground motion record [12].

As an example, Fig. 2 shows, for bilinear cyclic behavior, the 44 individual collapse capacity spectra for the 44 earthquake records of FEMA P-695 far-field ground motion set (FEMA P-695 [18]) with assigned structural parameters  $\theta - \alpha = 0.20$  and  $\zeta = 0.05$ . Additionally, the corresponding median, 16th and 84th percentile spectra are also displayed. Note that the records of the FEMA P-695 set originate from severe seismic events of magnitude between 6.5 and 7.6 and closest distance to the fault rupture larger than 10 km. Thereby, only strike-slip and reverse sources are considered. The 44 records of this set were recorded on NEHRP site classes C (soft rock) and D (stiff soil). For further details see FEMA P-695 [18]. Note that in [12] the FEMA P-695 ground motion set is referred to as ATC63-FF set.

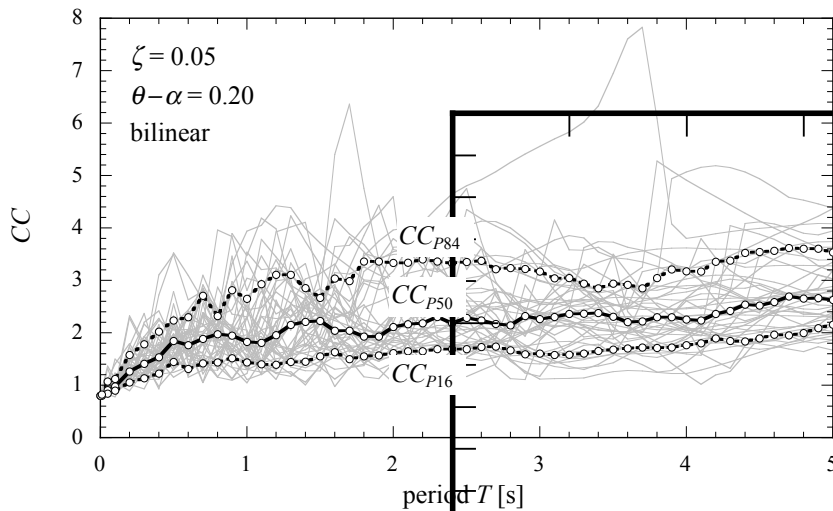


Fig. 2. Individual record dependent collapse capacity spectra for each record of the FEMA P-695 set. Corresponding median, 16th and 84th percentile spectra for bilinear hysteretic loop. Structural properties as defined in the figure

For the earthquake records of this set, in [12] collapse capacity spectra have been derived considering various damping coefficients, negative post-yield stiffness ratios, and hysteretic loops. In Fig. 3 each line with discrete circles represents graphically one median collapse capacity spectrum. The spectra of this figure were computed for 5% viscously damped SDOF systems with a bilinear cyclic behavior. Each graph of Fig. 3 refers to a specific negative slope of the post-tangent stiffness ratio  $\theta - \alpha$ . In particular, results for  $\theta - \alpha = 0.04, 0.06, 0.10, 0.20,$  and  $0.80$  are depicted. Naturally, for a fixed structural period  $T$  the collapse capacity is smaller the larger the negative slope  $\theta - \alpha$ . Furthermore, it can be seen that the collapse capacity depends on the initial structural period  $T$ . A general trend to larger collapse capacities with growing period  $T$  is readily observed. The period dependency of the collapse capacity is more pronounced for smaller values of  $\theta - \alpha$  [12].

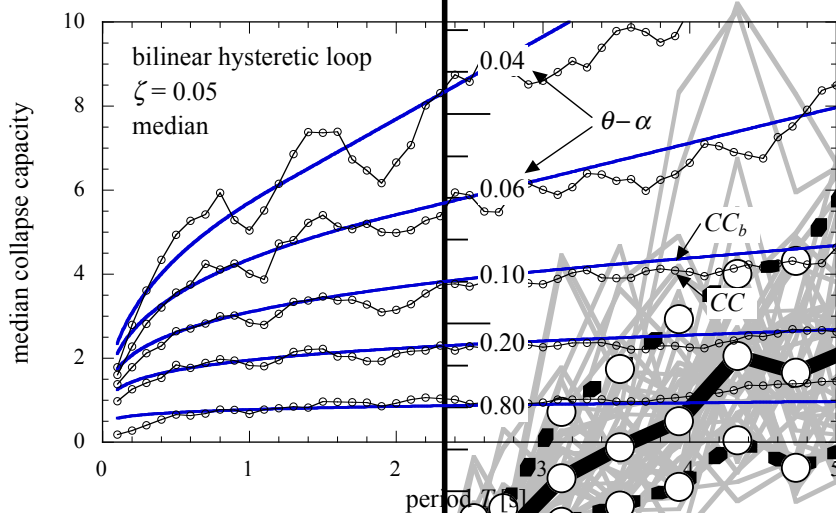


Fig. 3. Median collapse capacity spectra for various negative post-yield stiffness ratios  $\theta - \alpha$  based on the FEMA P-695 ground motion set, bilinear hysteretic loop, and 5% viscous damping (lines with discrete circles) and corresponding design collapse capacity spectra (solid lines) [12]

The curves shown in Fig. 3 might create the misleading perception that in a real structure the collapse capacity increases with period. As discussed in [11] the opposite holds true. In a real structure in general the collapse capacity tends to decrease the longer the fundamental period is, or in other words, the more

flexible the structure is. Furthermore, in many tall (long period) buildings in the bottom stories of the structure the stability coefficient in the inelastic range is usually much larger than the elastic stability coefficient. Thus, when the collapse capacity spectra of Fig. 3 are applied one has to interpolate between the various presented curves as the period of the structure becomes longer because simultaneously the stability coefficient is increased. Moreover, a lower collapse capacity for long period structures does not necessarily result in a larger probability of failure because the seismic hazard decreases for such systems.

### c) Design collapse capacity spectra – original version

In [12] analytical expressions for collapse capacity spectra of 5% viscously damped bilinear SDOF models have been derived via non-linear regression analyses. These spectra, which are based on the FEMA P-695 ground motion set, are referred to as “base case” design collapse capacity spectra (denoted as  $CC_b$ ). They read as

$$CC_b(T, \theta - \alpha) = \begin{cases} qT^p & T \leq T_1 \\ qT_1^p + qpT_1^{(p-1)}(T - T_1) & T > T_1 \end{cases} \quad (5)$$

with

$$q(\theta - \alpha) = \frac{2}{3}(\theta - \alpha)^{-2/3}, \quad p(\theta - \alpha) = \frac{3}{100}(\theta - \alpha)^{-7/10} + \frac{1}{10} \quad (6)$$

$$T_1(\theta - \alpha) = \begin{cases} 40(\theta - \alpha) - \frac{2}{5} & (\theta - \alpha) \leq 0.10 \\ \frac{18}{5} & (\theta - \alpha) > 0.10 \end{cases} \quad (7)$$

In Fig. 3 exemplarily solid lines depict a set of smooth base case median design collapse capacity spectra.

In [12] the impact of parameters, which differ from the base case, such as viscous damping coefficients different from 5%, and/or pinching or peak-oriented cyclic behavior on  $CC_b$  is considered via two independent multipliers, i.e. coefficient  $\psi_\zeta$  for damping and coefficient  $\psi_m$  for the hysteretic loop,

$$CC_d(T, \theta - \alpha, \zeta, \bar{f} - \mu) = \psi_\zeta \psi_m CC_b \quad (8)$$

For brevity, the expressions for the coefficients  $\psi_\zeta$  and  $\psi_m$  are not repeated here.

However, since in reality for some parameter combinations the impact of viscous damping and hysteretic material behavior different from the base case on the collapse capacity cannot be captured by these independent coefficients  $\psi_\zeta$  and  $\psi_m$  appropriately, relation (8) leads to collapse capacity predictions that are far off the actual values derived via IDAs. Thus, the aim of the presented paper is to improve the analytical relations given in Eqs. (5) to (8) considering the interaction of damping and hysteretic behavior on the design collapse capacity. Thereby, new functional relations will be derived by means of regression analysis, without further use of the coefficients  $\psi_\zeta$  and  $\psi_m$ . The refined design collapse capacity spectra derived subsequently are denoted by  $\widehat{CC}$  to distinguish them from their “original” counterpart  $CC_d$ .

### 3. REFINED DESIGN COLLAPSE CAPACITY SPECTRA

#### a) Underlying data for the multiple regression analysis

In this paper multiple regression analyses were performed with one dependent variable, i.e. the collapse capacity, and three regressors, i.e. the structural period of vibration  $T$ , the damping coefficient  $\zeta$  and the negative post-yield stiffness ratio  $\theta - \alpha$ . Specifically, median collapse capacities and the corresponding 16th, and 84th percentiles for 52 discrete initial structural periods  $T$ , seven discrete post-yield stiffness ratios  $\theta - \alpha$ , and seven discrete damping coefficients  $\zeta$ , i.e.

- $T_i = 0.01s, 0.05s, 0.1s, 0.2s, 0.3s, 0.4s, \dots, 5.0s \quad i = 1, \dots, 52$
- $(\theta - \alpha)_j = 0.04, 0.06, 0.08, 0.1, 0.2, 0.4, 0.8 \quad j = 1, \dots, 7$
- $\zeta_k = 0.05, 0.04, 0.03, 0.02, 0.01, 0.005, 0 \quad k = 1, \dots, 7$

provide the basis for the refined analytical approximation of the collapse capacity (denoted as  $\widehat{CC}$ ). In total these are  $52 \cdot 7 \cdot 7 = 2548$  discrete values of  $CC_{P50}$ ,  $CC_{P16}$  and  $CC_{P84}$  each, both for bilinear and peak oriented hysteretic cyclic behavior.

Note that not all investigated parameter combinations may be present in realistic physical systems. For example, it is very unlikely that stiff systems with periods  $T$  up to (at least)  $0.2s$  are vulnerable to P-delta induced collapse. On the other hand, a well-designed structure would never exhibit a negative post-yield stiffness ratio of  $\theta - \alpha = 0.8$ . It is, however, of scientific interest to understand the collapse capacity for these extreme cases at the parameter boundaries.

#### b) Shape function for the multiple regression analysis

The multiple linear regression analyses are based on the non-linear shape function

$$\widehat{CC} = A + BT + D e^{-c_1 T} + [1 - (\theta - \alpha) - A - D] e^{-c_2 T} \quad (9)$$

identified from upfront inspection of the underlying discrete raw data and the procedure described in the subsequent subsection 3.c of this paper. Coefficients  $A$ ,  $B$  and  $D$  are themselves shape functions, depending on the negative post-yield stiffness ratio  $\theta - \alpha$  and damping coefficient  $\zeta$ :

$$A = A_1 + A_2 \zeta, \quad B = B_1 + B_2 \zeta \quad (10)$$

$$D = D_1 + D_2 \zeta + D_3 (\theta - \alpha) + D_4 \zeta (\theta - \alpha) \quad (11)$$

$D_1$ ,  $D_2$ ,  $D_3$  and  $D_4$  are constants, whereas  $A_1$ ,  $A_2$ ,  $B_1$  and  $B_2$  are power functions with respect to  $\theta - \alpha$ :

$$A_1 = A_{11} + A_{12} (\theta - \alpha)^{g_1} + A_{13} (\theta - \alpha)^{g_2}, \quad A_2 = A_{21} + A_{22} (\theta - \alpha)^{h_1} + A_{23} (\theta - \alpha)^{h_2} \quad (12)$$

$$B_1 = B_{11} + B_{12} (\theta - \alpha)^{j_1}, \quad B_2 = B_{21} + B_{22} (\theta - \alpha)^{k_1} + B_{23} (\theta - \alpha)^{k_2} \quad (13)$$

The computation of the coefficients and exponents in Eqs. (10) to (13) is an elaborate task that is explained in detail in the following subsection 3.c.

#### c) Mathematical procedure of the multiple regression analysis

The regression analyses are performed in several steps. Thereby, the a priori unknown coefficients of Eq. (9) are adjusted to meet the constraint  $\widehat{CC} = 1 - (\theta - \alpha)$  for  $T = 0$ , compared with Eq. (4). Due to this constraint the applied regressions are with fixed intercept.

At the beginning of the analysis a shape function, which is already anticipated in Eq. (9), must be found. Thereby, in a first step the collapse capacity is approximated by a linear function with respect to the period  $T$  in the range  $0.5s \leq T \leq 5s$  :

$$\widehat{CC} = a + bT \tag{14}$$

Coefficients  $a$  and  $b$  are computed for each discrete collapse capacity based on  $(\theta - \alpha)_j$  ( $j = 1, \dots, 7$ ) and  $\zeta_k$  ( $k = 1, \dots, 7$ ) by linear regression with respect to the period  $T$ , resulting in the 49 discrete coefficients denoted by  ${}_{jk}a$  and  ${}_{jk}b$ . Then, for each parameter  $(\theta - \alpha)_j$  these discrete quantities are approximated by a linear function with respect to  $\zeta$ , leading to the coefficients  ${}_ja$  and  ${}_jb$  :

$${}_ja = {}_ja_1 + {}_ja_2\zeta, \quad {}_jb = {}_jb_1 + {}_jb_2\zeta \tag{15}$$

These coefficients are continuous with respect to  $\zeta$ , however, still discrete with respect to  $(\theta - \alpha)_j$ . In Fig. 4 for  $(\theta - \alpha)_{j=5} = 0.20$  discrete coefficients  ${}_{j=5,k}a$ ,  ${}_{j=5,k}b$ , and their discrete/continuous counterparts  ${}_{j=5}a$ ,  ${}_{j=5}b$  are depicted for the regression analysis applied to the median collapse capacity of an SDOF system with bilinear cyclic behavior.

Subsequently, another linear regression analysis is applied to determine sub-coefficients  ${}_ja_1$ ,  ${}_ja_2$ ,  ${}_jb_1$  and  ${}_jb_2$ . These sub-coefficients are approximated by continuous power functions with respect to  $\theta - \alpha$ , denoted as  $a_1$ ,  $a_2$ ,  $b_1$  and  $b_2$ ,

$$a_1 = a_{11} + a_{12}(\theta - \alpha)^{g_1} + a_{13}(\theta - \alpha)^{g_2}, \quad a_2 = a_{21} + a_{22}(\theta - \alpha)^{h_1} + a_{23}(\theta - \alpha)^{h_2} \tag{16}$$

$$b_1 = b_{11} + b_{12}(\theta - \alpha)^{j_1}, \quad b_2 = b_{21} + b_{22}(\theta - \alpha)^{k_1} + b_{23}(\theta - \alpha)^{k_2} \tag{17}$$

The exponents of Eqs. (16) and (17), i.e.  $g_1$ ,  $g_2$ ,  $h_1$ ,  $h_2$ ,  $j_1$ ,  $k_1$ ,  $k_2$ , as well as sub-sub-coefficients  $a_{rs}$ ,  $b_{rs}$  ( $r = 1, 2$ ;  $s = 1, 2, 3$ ) are determined by non-linear curve fitting of the discrete data. As an example, Fig. 5 shows, additionally, the discrete quantities  ${}_ja_1$ ,  ${}_ja_2$ ,  ${}_jb_1$  and  ${}_jb_2$ , also the continuous counterparts, i.e. Eqs. (16) and (17), for approximating the median collapse capacity of SDOF systems with bilinear constitutive behavior.

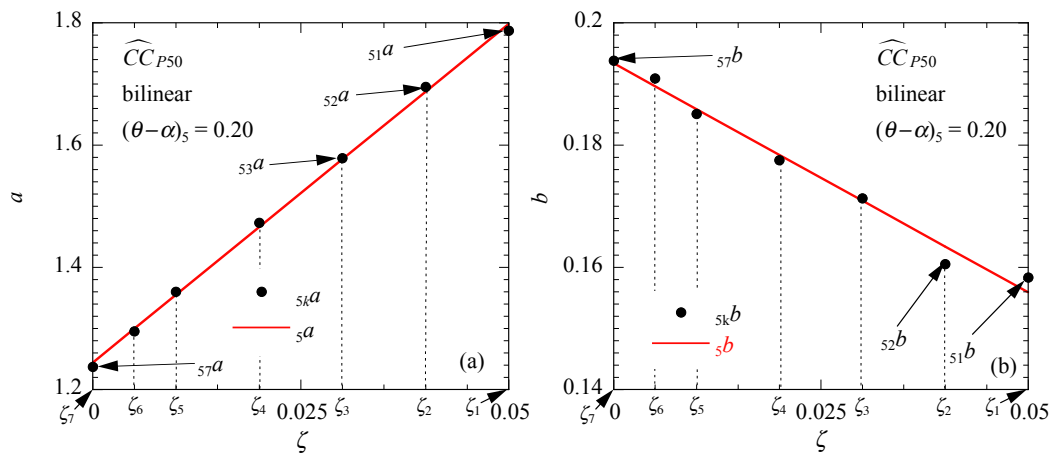


Fig. 4. Regression coefficients  $a$  and  $b$  exemplarily for the median collapse capacity of an SDOF system with bilinear hysteretic behavior and  $\theta - \alpha = 0.20$ , plotted against the viscous damping coefficient  $\zeta$ . Discrete values and corresponding regression line

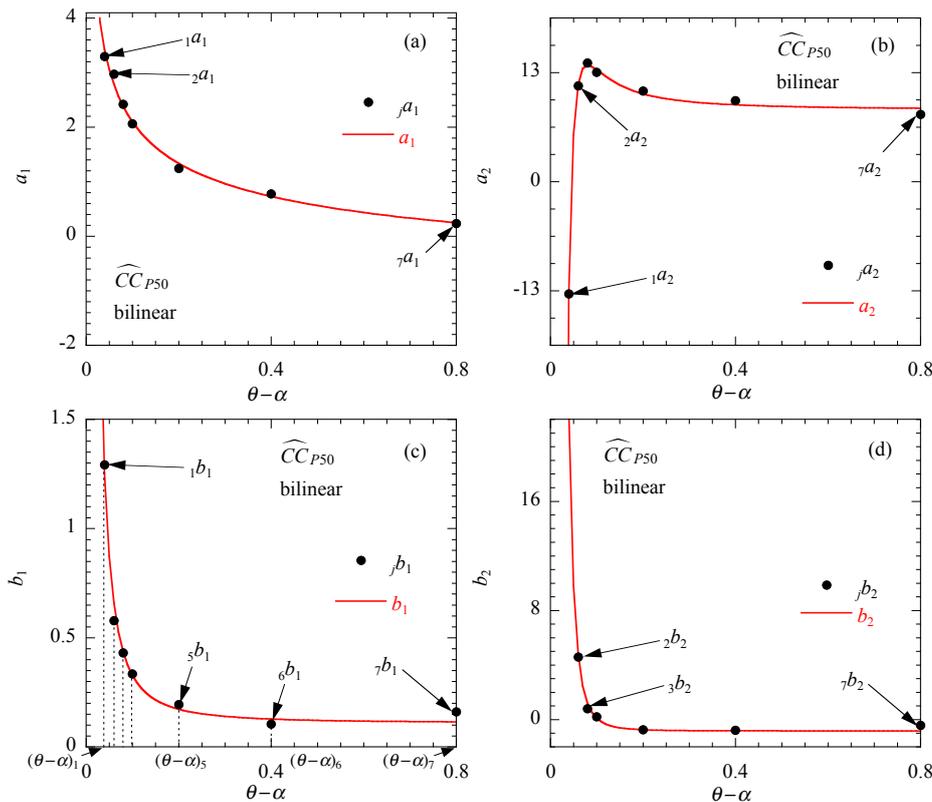


Fig. 5. Regression coefficients  $a_1, a_2, b_1, b_2$  exemplarily for the median collapse capacity of an SDOF system with bilinear hysteretic behavior, plotted as function of the post-yield stiffness ratio  $\theta - \alpha$ . Discrete values and corresponding regression line

In a further step, two exponential functions are added to  $\widehat{CC}$  in order to obtain a better fit for the low period range  $0 \leq T \leq 0.5s$ , leading to the expression of the non-linear shape function Eq. (9). Constants  $c_1$  and  $c_2$  are the outcome of non-linear curve fitting as well.

In conclusion, the result of the intermediate regression analyses so far is the shape function Eq. (9), and the exponents  $g_1, g_2, h_1, h_2, j_1, k_1, k_2, c_1$  and  $c_2$ .

Having thus determined the shape function, unknown constants  $D_l$  ( $l = 1, \dots, 4$ ) and coefficients  $A_{rs}, B_{rs}$  ( $r = 1, 2; s = 1, 2, 3$ ), which show up in Eqs (11) to (13), are computed based on a final global linear regression applied to Eq. (9). The regression is performed employing the method of weighted least squares, minimizing the following sum of squares of the errors (SSE):

$$SSE = \sum_{i=1}^{52} \sum_{j=1}^7 \sum_{k=1}^7 w_{ijk} \left( \widehat{CC}(T_i, (\theta - \alpha)_j, \zeta_k) - CC(T_i, (\theta - \alpha)_j, \zeta_k) \right)^2 = \min \quad (18)$$

The weights  $w_{ijk}$  are selected to account for the importance of the accuracy in different ranges of  $T, \theta - \alpha$  and  $\zeta$ .

The resulting regression coefficients  $D_1, D_2, D_3, D_4, A_{rs}, B_{rs}$  ( $r = 1, 2; s = 1, 2, 3$ ) and exponents  $c_1, c_2, g_1, g_2 \dots$  are listed in Table A1 of the Appendix. They are specified for the median, 16th and 84th collapse capacity spectra, both for bilinear and peak-oriented hysteretic behavior.

Inserting these coefficients into Eq. (9) defines fully enhanced analytical expressions of the collapse capacity spectra. As an example, Fig. 6 shows the median collapse capacity spectrum for a bilinear SDOF system with 2% damping and a negative post-yield stiffness ratio of  $\theta - \alpha$ . A detailed evaluation of these spectra is provided in section d.

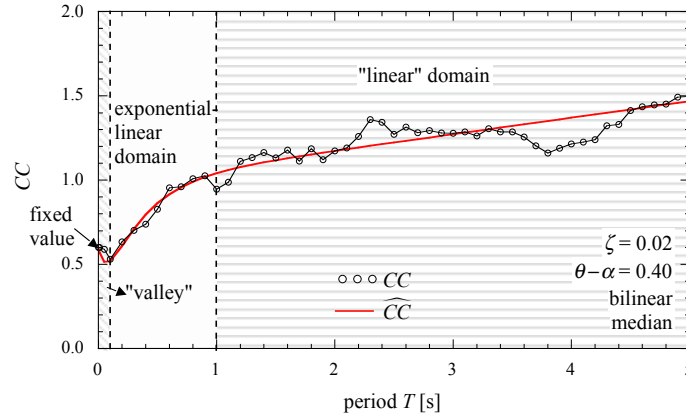


Fig. 6. Different domains of refined design collapse capacity spectra

**d) Domains of analytical collapse capacity spectra**

The analytical collapse capacity spectra are composed of four domains, as shown exemplarily in Fig. 6:

- Rigid system ( $T = 0$ ): For rigid systems the collapse capacity is given by the deterministic expression Eq. (4), i.e. record independent, and thus, the record-to-record dispersion of the collapse capacity is zero.
- The valley: The graph of  $\widehat{CC}$  exhibits, for large negative stiffness ratios  $\theta - \alpha$ , a valley for short period systems with approximately  $T = 0.05s$  (see Fig. 5). These combinations of the structural parameters that lead to the valley are, however, unlikely for real structures. The shape of the valley is primarily governed by coefficient  $D$  in Eq. (9). This valley is more pronounced if the damping coefficient  $\zeta$  is small.
- The exponential-linear domain: For short to medium period systems  $0.1s \leq T \leq 1.0s$  the first exponential term in Eq. (9) turns out to be negligibly small. Thus, the collapse capacity can be expressed by  $\widehat{CC} \approx A + BT + [1 - (\theta - \alpha) - A - D]e^{-c_2 T}$ .
- The “linear” domain: The collapse capacity of medium to long period systems, i.e.  $1.0s \leq T \leq 5.0s$ , is almost linear with respect to the period  $T$ :  $\widehat{CC} \approx A + BT$ . In this case the contribution of exponential terms is very small.

**4. EVALUATION OF REFINED DESIGN COLLAPSE CAPACITY SPECTRA**

As a result, analytical design collapse capacity spectra for two different hysteretic models (bilinear and a peak-oriented hysteretic model), and three representative statistical quantities of the collapse capacity, i.e. its median, 16th and 84th percentile, based on different values of the characteristic structural parameters of SDOF systems are now available.

Subsequently, the proposed regression model  $\widehat{CC}$  is set in contrast to the original regression model  $CC_d$ , Eq. (8), presented in [12], and the improvement is quantified. Since the regression is with fixed intercept, the coefficient of determination  $R^2$  cannot be used as a measure of goodness of fit [19]. Rather, in this study the mean square error MSE is employed for the considered design spectrum for each discrete value  $(\theta - \alpha)_j$  and  $\zeta_k$ ,

$$MSE = \frac{1}{52} \sum_{i=1}^{52} \left[ \widehat{CC}(T_i, (\theta - \alpha)_j, \zeta_k) - CC(T_i, (\theta - \alpha)_j, \zeta_k) \right]^2 \tag{19}$$

as recommended by Montgomery et al. [20]. This measure quantifies the average squared deviation of the actual collapse capacities from those obtained from the regression analysis. The  $MSE_{\widehat{CC}}$  values based on the new analytical expressions are compared with the  $MSE_{CC_d}$  values that correspond to the existing analytical equations, both derived according to Eq. (19). Furthermore, a relative improvement index  $I$  is defined:

$$I = 1 - \frac{MSE_{\widehat{CC}}}{MSE_{CC_d}} \tag{20}$$

Note that the closer index  $I$  to unity the better is the relative improvement.

Exemplarily, Fig. 7 shows the enhanced (solid lines) and the original (dashed lines) analytical design median, 16th and 84th percentile spectra, respectively, and the corresponding outcomes from IDAs (circles) for both considered hysteretic models, for selected assigned post-yield stiffness ratios  $\theta - \alpha = 0.10, 0.20$  and  $0.40$ , and viscous damping  $\zeta = 0.05$ . In general, SDOF systems with peak-oriented hysteretic loop proved to be less vulnerable to the collapse due to P-delta than those with a bilinear hysteretic model [16]. This observation is also consistent with pinching material behavior compared to the bilinear one [12]. The improvement of the proposed relations can already be observed visually. In particular, in the short period range all refined spectra lead to a more appropriate approximation of the outcomes from IDAs. The refined 84th percentile spectra show a better performance for both material models.

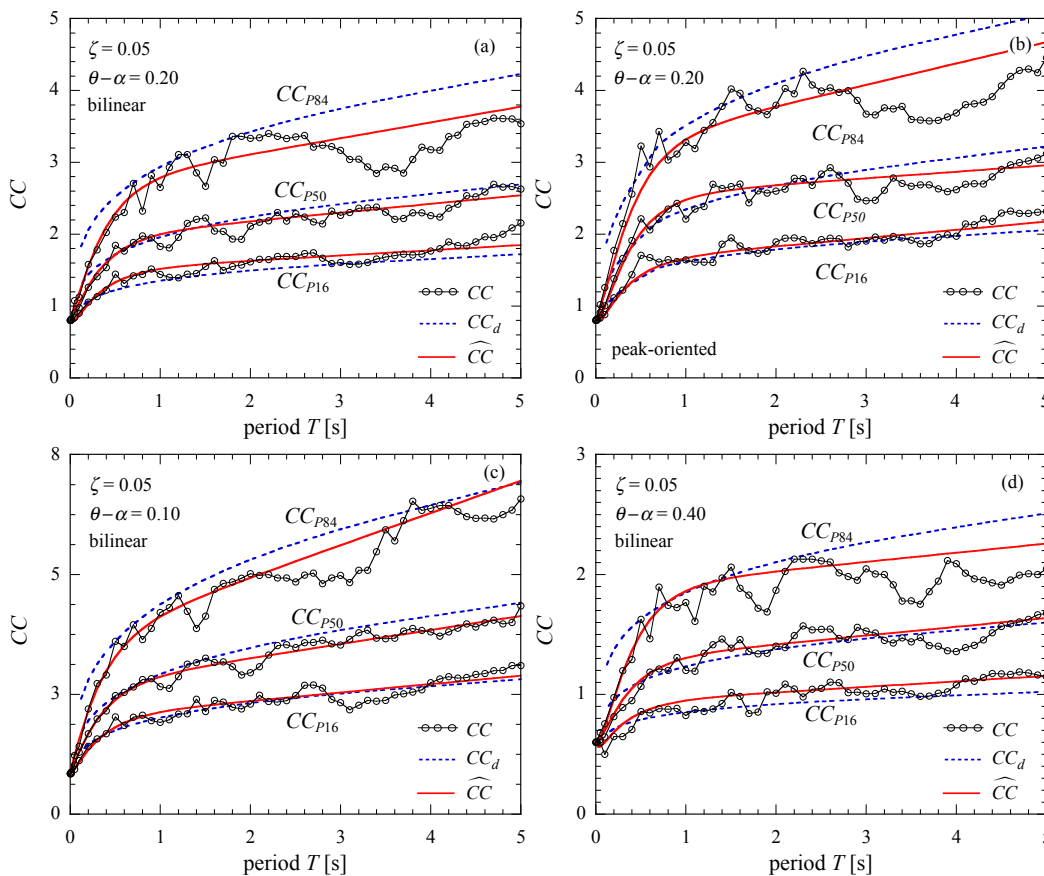


Fig. 7. Median, 16th and 84th percentile collapse capacity spectra for (a), (c), (d) bilinear and (b) peak-oriented hysteretic behavior based on the FEMA P-695 ground motion set. 5% damping. (a), (b)  $\theta - \alpha = 0.20$ ; (c)  $\theta - \alpha = 0.10$ , (d)  $\theta - \alpha = 0.40$ . Lines with discrete circles: outcomes from IDAs. Solid lines: refined design spectra. Dashed lines: original design spectra

In Tables 1 and 2 improvement index  $I$  is specified for several example problems. In all examples of Table 1 damping is 5%, in those of Table 2 damping is 2%. For clarification, in these tables the MSE values are also listed, because index  $I$  is a *relative* measure of improvement only. The outcomes for the collapse spectra depicted in Fig. 7 are shown in the third, fourth and fifth block of Table 1. It can be seen that for these structural configurations the MSE of most statistical quantities drops significantly, and thus the improvement index is quite large. For some other structural configurations index  $I$  is relatively small (i.e. close to zero). However, this is only the case if the MSE of the original spectrum is already small, and thus no further significant improvement can be gained. It is readily observed that in most cases the MSE values for peak-oriented systems are larger than those for bilinear ones. This is a result of the conducted regression procedure, where initially the shape functions were adjusted to the data of the bilinear systems. Then, in an effort to provide a uniform representation of collapse capacity spectra, for peak-oriented systems the same shape functions were used, however, determining the coefficients and exponents based on the data for peak-oriented systems. The results of Tables 1 and 2 provide evidence of the substantial improvement of the proposed relation, Eq. (9), compared to the original one, Eq. (8).

Table 1. Mean square error values for the existing relations  $MSE_{CC_d}$  and the proposed  $MSE_{\widehat{CC}}$ . Corresponding improvement index  $I$  for several specified structural configurations. Damping  $\zeta = 0.05$

	Bilinear hysteretic loop			Peak-oriented hysteretic loop		
	$MSE_{CC_d}$	$MSE_{\widehat{CC}}$	$I$	$MSE_{CC_d}$	$MSE_{\widehat{CC}}$	$I$
$\theta - \alpha = 0.04$						
P16	0.858	0.130	0.848	0.907	0.290	0.680
P50	2.269	1.978	0.128	0.800	0.722	0.098
P84	2.206	1.005	0.544	3.980	1.768	0.556
$\theta - \alpha = 0.06$						
P16	0.109	0.047	0.569	0.138	0.088	0.362
P50	0.162	0.101	0.377	0.446	0.418	0.063
P84	1.120	0.474	0.577	1.445	1.326	0.082
$\theta - \alpha = 0.10$						
P16	0.029	0.025	0.138	0.038	0.038	0.000
P50	0.078	0.017	0.782	0.174	0.110	0.368
P84	0.363	0.148	0.592	0.488	0.201	0.588
$\theta - \alpha = 0.20$						
P16	0.024	0.009	0.625	0.019	0.010	0.474
P50	0.026	0.011	0.577	0.055	0.021	0.618
P84	0.304	0.067	0.780	0.406	0.141	0.653
$\theta - \alpha = 0.40$						
P16	0.010	0.004	0.574	0.010	0.005	0.521
P50	0.009	0.007	0.215	0.009	0.008	0.063
P84	0.110	0.034	0.691	0.102	0.063	0.379
$\theta - \alpha = 0.80$						
P16	0.017	0.005	0.706	0.019	0.010	0.474
P50	0.044	0.021	0.523	0.046	0.009	0.804
P84	0.063	0.045	0.286	0.062	0.032	0.484

Table 2. Mean square error values for the existing relations  $MSE_{CC_d}$  and the proposed  $MSE_{\widehat{CC}}$ . Corresponding improvement index  $I$  for several specified structural configurations. Damping  $\zeta = 0.02$

	Bilinear hysteretic loop			Peak-oriented hysteretic loop		
	$MSE_{CC_d}$	$MSE_{\widehat{CC}}$	$I$	$MSE_{CC_d}$	$MSE_{\widehat{CC}}$	$I$
$\theta - \alpha = 0.04$						
P16	0.257	0.158	0.386	0.203	0.148	0.269
P50	1.243	0.824	0.337	1.020	0.663	0.350
P84	1.717	0.749	0.564	4.472	1.615	0.639
$\theta - \alpha = 0.06$						
P16	0.065	0.056	0.133	0.067	0.047	0.301
P50	0.104	0.077	0.265	0.396	0.383	0.034
P84	0.684	0.345	0.496	0.921	0.864	0.063
$\theta - \alpha = 0.10$						
P16	0.017	0.014	0.163	0.035	0.017	0.504
P50	0.097	0.014	0.861	0.213	0.082	0.614
P84	0.501	0.100	0.801	0.707	0.210	0.703
$\theta - \alpha = 0.20$						
P16	0.011	0.006	0.449	0.013	0.008	0.379
P50	0.023	0.007	0.683	0.040	0.020	0.500
P84	0.318	0.065	0.794	0.317	0.128	0.597
$\theta - \alpha = 0.40$						
P16	0.004	0.004	0.145	0.006	0.004	0.321
P50	0.007	0.005	0.241	0.009	0.008	0.144
P84	0.075	0.026	0.653	0.073	0.051	0.304
$\theta - \alpha = 0.80$						
P16	0.013	0.005	0.603	0.014	0.006	0.539
P50	0.033	0.024	0.276	0.033	0.017	0.496
P84	0.087	0.062	0.290	0.085	0.056	0.344

Figure 8 visualizes a set of the median, 16th and 84th collapse capacity spectra for discrete values of  $\theta - \alpha$  equal to 0.04, 0.06, 0.10, 0.20 and 0.80. Damping is fixed at  $\zeta = 0.05$ , bilinear cyclic behavior is considered. The MSE and the index  $I$  for these cases is also listed in Table 1. In this Fig. improved design collapse capacity spectra, as well as the underlying data from IDAs are depicted.

From the three subplots some mainstreams can be observed. Firstly, as the slope of negative stiffness becomes steeper (i.e.  $\theta - \alpha$  becomes larger), the SDOF system is more vulnerable to collapse. The collapse capacity decreases, and therefore, the structure should be designed stronger in order to avoid collapse. In particular, for extreme values of  $\theta - \alpha$  the structure should be designed not to deform beyond the elastic region. Furthermore, it can be seen that the collapse capacity depends on the initial structural period  $T$  [12]. The period dependence of collapse capacity  $CC$  for mild  $\theta - \alpha$  is more pronounced.

In earthquake engineering the prediction of the structural response is usually based on a viscous damping coefficient of  $\zeta = 0.05$ . However, for some structures such as slightly damped steel towers smaller values of damping are more meaningful. Therefore, in Fig. 9 the effect of different damping coefficients ( $\zeta = 0.00, 0.02, 0.05$ ) for both hysteretic models and the two regression lines  $\widehat{CC}$ ,  $CC_d$  are depicted. The considered post-yield stiffness ratios  $\theta - \alpha$  are 0.10, 0.20 and 0.40, respectively. Naturally, systems with lower values of viscous damping coefficients  $\zeta$  exhibit larger deformation, resulting in smaller collapse capacities. The enhanced linear regression model provides improved regression lines with a rate of improvement  $I$  of the MSE of 50% and more in most of the cases, apart from the peak-oriented model with  $\zeta = 0.05$ . In the cases, where  $I$  is smaller, the mean square error of the original regression model is already very small, compared with Tables 1 and 2.

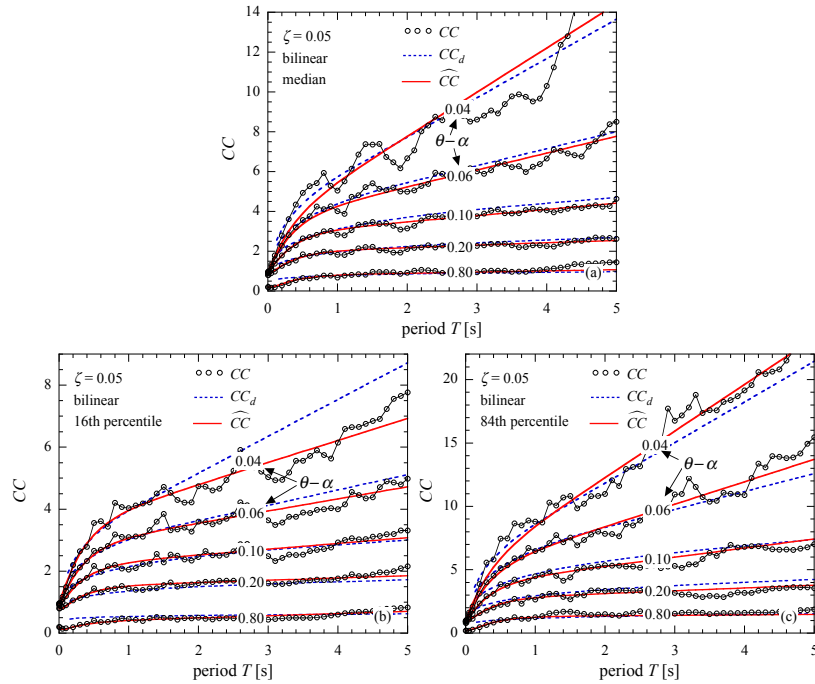


Fig. 8. Sets of (a) median, (b) 16th percentile, and (c) 84th percentile collapse capacity spectra for bilinear hysteretic loop,  $\zeta = 0.05$ , based on the FEMA P-695 ground motion set. Various negative post-yield ratios  $\theta - \alpha$ . Lines with discrete circles: outcomes from IDAs. Solid lines: refined design spectra. Dashed lines: original design spectra

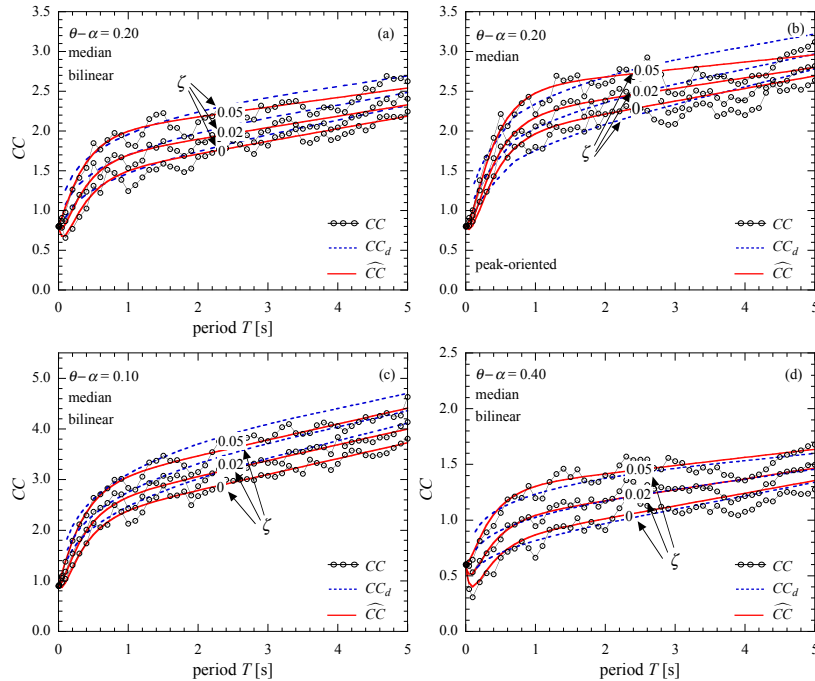


Fig. 9. Median collapse capacity spectra for (a), (c), (d) bilinear and (b) peak-oriented hysteretic loop based on the FEMA P-695 ground motion set. Three different viscous damping values  $\zeta$ . (a), (b)  $\theta - \alpha = 0.20$ ; (c)  $\theta - \alpha = 0.10$ ; (d)  $\theta - \alpha = 0.40$ . Lines with discrete circles: outcomes from IDAs. Solid lines: refined design spectra. Dashed lines: original design spectra

Table 3 illustrates, for both hysteretic models and damping coefficients  $\zeta$  of 0.05 and 0.02, the mean improvement index (denoted as  $\bar{I}$ ) for the 16th, 50th and 84th percentiles derived from all considered post-yield stiffness ratios  $\theta - \alpha$  ( $0.04 \leq \theta - \alpha \leq 0.80$ ) and from the “most common” ones  $\theta - \alpha$

( $0.08 \leq \theta - \alpha \leq 0.40$ ). Also these results provide evidence of significant improvement of the proposed relations.

Table 3. Mean improvement index  $\bar{I}$  of the mean square error

Bilinear hysteretic loop				
	$\zeta = 0.05$		$\zeta = 0.02$	
	$0.04 \leq (\theta - \alpha) \leq 0.8$	$0.08 \leq (\theta - \alpha) \leq 0.4$	$0.04 \leq (\theta - \alpha) \leq 0.8$	$0.08 \leq (\theta - \alpha) \leq 0.4$
$\bar{I}_{P16}$	0.50	0.34	0.31	0.26
$\bar{I}_{P50}$	0.47	0.57	0.50	0.66
$\bar{I}_{P84}$	0.56	0.63	0.62	0.75
Peak-oriented hysteretic loop				
	$\zeta = 0.05$		$\zeta = 0.02$	
$\bar{I}_{P16}$	0.40	0.31	0.42	0.46
$\bar{I}_{P50}$	0.32	0.31	0.33	0.37
$\bar{I}_{P84}$	0.42	0.46	0.40	0.44

Collapse fragility curves that incorporate aleatory uncertainty due to record-to-record variability can be obtained by ordering the collapse capacities for FEMA P-695 record set, as shown exemplarily in Fig. 10. A reduced dispersion in case of bilinear SDOF models is readily observed for all considered examples with periods  $T = 0.1s, 1s, 2s, 4s$ , assigned post-yield stiffness ratio of  $\theta - \alpha = 0.20$ , and assigned damping of  $\zeta = 0.05$  and  $\zeta = 0.02$ , respectively. This reduction is a general trend for the entire range of  $T$  and  $\theta - \alpha$ . It is readily observed that the proposed enhanced regression model (solid lines) leads to a pronounced better fitting of the sorted collapse fragility curves (stepped line) for all the given periods in comparison with the original regression model (dashed lines).

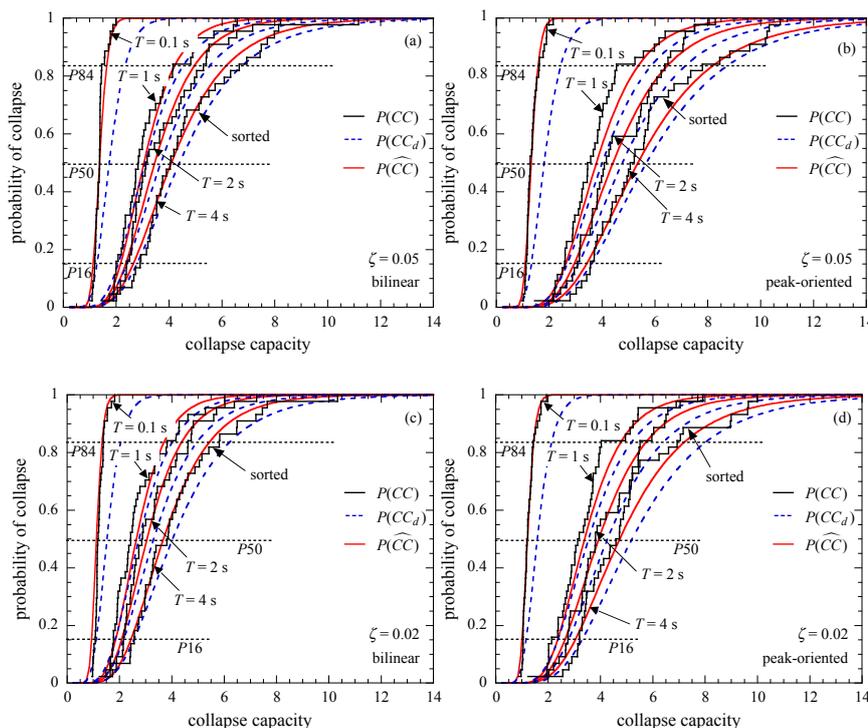


Fig. 10. Collapse fragility curves for (a), (c) bilinear and (b), (d) peak-oriented hysteretic loop based on the FEMA P-695 ground motion set. Various values of fundamental periods  $T$ .  $\theta - \alpha = 0.20$ . (a), (b)  $\zeta = 0.05$ ; (c), (d)  $\zeta = 0.02$ . Stepped lines: sorted collapse capacity from IDAs. Solid lines: refined regression analysis. Dashed lines: original regression analysis

## 6. CONCLUSION

Refined design median, 16th and 84th percentile collapse capacity spectra for both bilinear and peak-oriented hysteretic constitutive model and their analytical expressions were derived via a set of multiple linear regression analyses. Thereby, the median, 16th and 84th percentile, respectively, collapse capacity of single-degree-of-freedom systems served as the dependent variable, and the structural period of vibration, the viscous damping coefficient, and the post negative stiffness ratio as the three regressors. The proposed regression model is compared with an existing one from a previous study. It is shown that the improvement index  $I$  increases up to 85%, and the absolute values of mean square error are reduced significantly in most of the cases. The refined regression model improves the already existing collapse capacity spectra with large mean squared values, provides a better fit for short and large period systems, and leads to a more appropriate prediction of the 16th and 84th percentile collapse capacity spectra.

Refined design collapse capacity spectra are a useful, easily applicable and accurate tool for the prediction of the collapse capacity and their record-to-record uncertainties, with sufficient confidence, and the establishment of an adequate margin of safety against second-order effects.

**Acknowledgements:** S. Tsantaki and L. Wurzer conducted the research for this paper as students of the Doctoral School (FWF DK-PLUS) “Computational Interdisciplinary Modelling”, which is based at the University of Innsbruck and substantially funded by the Austrian Science Fund (FWF). The investigations of C. Jäger were partially funded by the Tyrolean Science Fund (TWF). This support is gratefully acknowledged.

## REFERENCES

1. Gupta, A. & Krawinkler, H. (2000). Dynamic P-delta effects for flexible inelastic steel structures. *Journal of Structural Engineering*, 126, 145-154.
2. Krawinkler, H., Zareian, F., Lignos, D. G. & Ibarra, L. F. (2009). Prediction of collapse of structures under earthquake excitations. *2nd International Conference on Computational Methods in Structural Dynamics and Earthquake Engineering*. (M. Papadrakakis, N.D. Lagaros, M. Fragiadakis eds). June 22-24, 2009, Rhodes, Greece, CD-ROM paper, paper no. CD449.
3. Jennings, P. C. & Husid, R. (1968). Collapse of yielding structures during earthquakes. *Journal of the Engineering Mechanics Division (ASCE)*, 94, 1045-1065.
4. Bernal, D. (1998). Instability of buildings during seismic response. *Engineering Structures*, 20, 496-502.
5. MacRae, G. A. (1994). P- $\Delta$  effects on single-degree-of-freedom structures in earthquakes. *Earthquake Spectra*, 10, 539-568.
6. Miranda, E. & Akkar, S. D. (2003). Dynamic instability of simple structural systems. *Journal of Structural Engineering*, 129, 1722-1726.
7. Vamvatsikos, D., Miranda, E. & Akkar, S. (2009). Estimating the dynamic instability of oscillators with non-trivial backbones. In: Proc. 2nd International Conference on Computational Methods in Structural Dynamics and Earthquake Engineering (COMPDYN 2009) (Papadrakakis M, Lagaros ND, Fragiadakis M, eds), June 22–24, 2009, Rhodes, Greece, CD-ROM paper, paper no. CD450.
8. Asimakopoulos, A. V., Karabalis, D. L. & Beskos, D. E. (2007). Inclusion of P- $\Delta$  effect in displacement-based seismic design of steel moment resisting frames. *Earthquake Engineering and Structural Dynamics*, 36, 2171-2188.
9. Villaverde, R. (2007). Methods to assess the seismic collapse capacity of building structures: State of the art. *Journal of Structural Engineering*, 133, 57-66.
10. Aydinoglu, M. N. & Fahjan, Y. M. (2003). A unified formulation of the piecewise exact method for inelastic seismic demand analysis including the P-delta effect. *Earthquake Engineering and Structural Dynamics*, 32, 871-890.

11. Adam, C. & Jäger, C. (2012). Simplified collapse capacity assessment of earthquake excited regular frame structures vulnerable to P-delta. *Engineering Structures*, 44, 159-173.
12. Adam, C. & Jäger, C. (2012). Seismic collapse capacity of basic inelastic structures vulnerable to the P-delta effect. *Earthquake Engineering and Structural Dynamics*, 41, 775-793.
13. Jäger, C. (2012). The collapse capacity spectrum methodology – a method for quick collapse capacity assessment of stability prone frame structures subjected to earthquake excitation (in German), PhD Thesis. University of Innsbruck.
14. Jäger, C. & Adam, C. (2013). Influence of collapse definition and near-field effects on collapse capacity spectra. *Journal of Earthquake Engineering*, 17, 859-878.
15. Vamvatsikos, D. & Cornell, C. A. (2002). Incremental dynamic analysis. *Earthquake Engineering and Structural Dynamics*, 31, 491-514.
16. Ibarra, L. & Krawinkler, H. (2005). Global collapse of frame structures under seismic excitations. PEER 2005/06. Pacific Earthquake Engineering Research Center, University of California at Berkeley, California.
17. Ibarra, L. & Krawinkler, H. (2011). Variance of collapse capacity of SDOF systems under earthquake excitations. *Earthquake Engineering and Structural Dynamics*, 40, 1299-1314.
18. FEMA P-695 (2009). Quantification of building seismic performance factors. Federal Emergency Management Agency, Washington D.C.
19. Hahn, G.J. (1977). Fitting regression models with no intercept term. *Journal of Quality Control*, 9, 56-61.
20. Montgomery, D. C., Peck, E. A. & Vining, G. G. (2012). Introduction to linear regression analysis. Fifth Edition. John Wiley & Sons, New York.

## APPENDIX

In Table A1 the regression coefficients are specified, which are the outcome of the applied multiple regression analyses.

Table A1. Regression coefficients for analytical median, 16th and 84th percentile collapse capacity spectra, both for bilinear and hysteretic behavior

	Bilinear hysteretic loop			Peak-oriented hysteretic loop		
	P50	P16	P84	P50	P16	P50
$A_{11}$	-1.5581	-0.5606	-1.2929	-3.5486	-1.6703	-1.4442
$A_{12}$	1.7272	0.6478	1.9835	3.6432	1.6884	2.3505
$A_{13}$	0	-0.0527	0	0	0	0
$A_{21}$	9.2175	14.4753	8.6889	16.8869	9.1459	6.9235
$A_{22}$	0.0863	-12.1523	0.1434	-0.4240	-0.0059	1.0436
$A_{23}$	-0.0042	0	-0.0056	-13.3478	-6.4376	0.0001
$B_{11}$	0.0959	0.0592	0.0549	0.0952	0.0532	-0.0424
$B_{12}$	0.0034	0.0108	0.0097	0.0025	0.0065	0.0355
$B_{21}$	-0.8232	-1.7801	-0.7455	-8.1363	-0.3062	-0.1885
$B_{22}$	0.0003	0.0071	0.0420	0.9482	0.0006	0.0019
$B_{23}$	0	2.0493	0	10.1838	0	0
$D_1$	0.6048	0.2416	0.6855	0.9284	0.4424	1.0770
$D_2$	-10.1506	-2.5458	-3.6266	-1.5098	-3.0968	-2.3823
$D_3$	-0.2564	0.0298	0.1121	-0.7373	-0.3145	-0.1078
$D_4$	8.6182	0.2894	-3.2410	-0.1670	1.6512	0.1966
$c_1$	15	30	10	10	20	8
$c_2$	3	3	3	3	3	3
$g_1$	-1/3	-1/2	-1/3	-1/4	-1/3	-1/3
$g_2$	0	1	0	0	0	0
$h_1$	-2	1	-2	-1	-2	-1
$h_2$	-3	0	-3	1	1	-3
$j_1$	-1.8	-1.2	-1.7	-2	-1.5	-7/5
$k_1$	-3.5	-2	-2	-1	-3	-3
$k_2$	0	1	0	1	0	0